www.lajss.org
Latin American Journal of Solids and Structures 4 (2007) 87–102

Analysis of in-layer strains in the low order MITC shell element

Victoria Vampa*

Dpto. de Matemática, Facultad de Ciencias Exactas, Universidad Nacional de La Plata, La Plata, Argentina

Abstract

In recent publications it was shown that the development of general shell elements using the method of mixed interpolation of tensorial components (MITC) is effective for general engineering applications. In particular, the MITC4 is a low order formulation that has been employed very successfully to approximate all deformation states of a shell. In this element, formulated in a convected coordinate system, separate interpolations for the shear terms are performed effectively.

However, in the bending-dominated case, the improvement of the MITC4 formulation with respect to the performance of the standard bilinear element is more important. In this paper a new shell element is presented where in-plane strains interpolation is based on a quadrilateral 2-D element, the QMITC. Numerical results for some test examples are presented and compared.

1 Introduction

In 1970 Ahmad, Irons and Zienkiewicz [1] introduced an isoparametric shell element with independent C^0 interpolations for displacement and rotations. From now on we will refer to this element as the A-I-Z shell element. The most relevant aspect of this element is that the interpolations functions require only C^o and introduce shear deformations. This elements are known as Reissner/Mindlin shell elements. Even though it seems to be desirable to include shear deformations for the analysis of thick shells, they cause the main numerical difficulty of the A-I-Z element: the locking phenomenon [2].

Most of the research developed in the area of shell elements since 1970 has been devoted to elements that while being based on the A-I-Z element try to overcome the locking problem, as the reduced/selective numerical integration schemes. However the introduction of spurious zero energy modes lowers the reliability of their numerical results. It has been shown that reduced and selective integration methods are equivalent to mixed formulations and drawbacks like the presence of spurious zero energy modes cannot be avoided except that reduced/selective integration schemes are used together with some stabilization procedures [12]. In 1980, Bathe and

*Corresp. author email: victoria@mate.unlp.edu.ar 12 Jun 2006; In revised form 31 Jan 2007

Dvorkin (see [3–6, 9, 10]) proposed the mixed interpolation tensorial components and circumvented the locking problem. These finite elements, the MITC, are very attractive, reliable and efficient.

In particular, the MITC4 is a low order shell element that performs well both in membrane-dominated and bending-dominated situations and a very good locking free behavior in the latter case can be observed [7].

The outline of the paper is at follows. In Section 2 we will review the A-I-Z shell element formulation, and the method of mixed interpolation of tensorial components (MITC) introduced by Bathe and Dvorkin [9]. In Section 3 we present a new shell element adapting the interpolations proposed in [11] for a 2D-quadrilateral element. Finally, in Section 4 we analyze the numerical behavior of the new element: we check convergence and present few test problems.

2 The MITC4 shell element

The general A-I-Z element (see Figure 1) is based on degenerating a 3D solid finite element. In order to describe its geometry we use [2]:

· The coordinates of the mid-surface nodes, $\underline{x}^k$,

· Director vectors at the nodes that approximate the shell normal at those points, $\underline{V}_n^k$,

· The position vector of any point inside the shell element, with natural coordinates (r_1, r_2, r_3), at any time (load level) t, is given by

$$ {}^t\underline{x} = h_k \, {}^t\underline{x}^k + \frac{r_3}{2} \; h_k \, a_k \, {}^t\underline{V}_n^k \tag{1} $$

where $t = 0$ represents the reference undeformed configuration.

In Eq. (1) the summation convention is used and:

h_k: 2D isoparametric interpolation function [2] corresponding to the k-th node

${}^t\underline{x}^k$: Cartesian coordinates of the k-th mid-surface node at time t,

a_k: thickness at the k-th node

${}^t\underline{V}_n^k$: director vector at node k, $\left|{}^t\underline{V}_n^k\right| = 1$.

The kinematic description implies the following hypotheses: the director vectors remain straight during the deformations (Naghdi shell model assumption, [7]); the thickness a_k remains constant during the deformations, hence only small strain conditions are considered.

For the point (r_1, r_2, r_3), substracting ${}^0\underline{x}$ from ${}^t\underline{x}$, and taking into account that the increment ${}^t\underline{V}_n^k - {}^0\underline{V}_n^k$ can be expressed in terms of the rotations, the incremental displacements $\underline{u}$ can be written [2]

$$ \underline{u} = h_k \; \underline{u}^k \; + \frac{r_3}{2} \; h_k \; a_k \; (-\alpha_k \; {}^0\underline{V}_2^k \; + \beta_k \; {}^0\underline{V}_1^k) \tag{2} $$

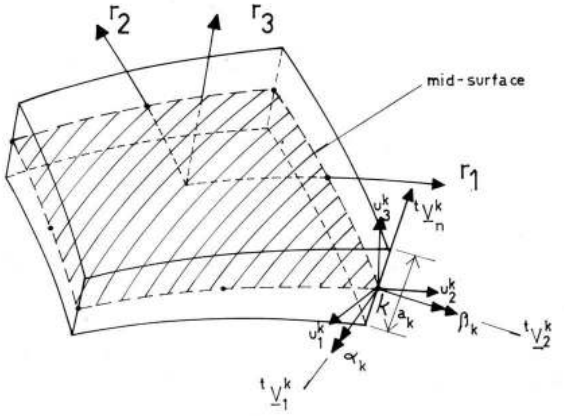


Figure 1: The A-I-Z shell element

where $\underline{u}^k$ is the k-th nodal incremental displacement, α_k and β_k are the incremental rotations of the director vector about ${}^0\underline{V}_1^k$ and ${}^0\underline{V}_2^k$ axes

$$ {}^0\underline{V}_1^k = \frac{\underline{e}_2 \times {}^0\underline{V}_n^k}{\left|\underline{e}_2 \times {}^0\underline{V}_n^k\right|} \tag{3} $$

$$ {}^0\underline{V}_2^k = {}^0\underline{V}_n^k \times {}^0\underline{V}_1^k \tag{4} $$

In this way ${}^0\underline{V}_1^k$ and ${}^0\underline{V}_2^k$ are unitary vectors orthogonal to ${}^0\underline{V}_n^k$ as it is shown in Figure 1, using a special definition of ${}^0\underline{V}_1^k$ and ${}^0\underline{V}_2^k$ in case ${}^0\underline{V}_n^k$ is parallel to the $y-axis$

Note that only 5 degrees of freedom are used for each shell element node (three corresponding to displacements u_i^k, $i = 1, 2, 3$, and two corresponding to rotations, α_k and β_k) and that the thickness of the element can vary and the element is in general non-flat.

In Figure 2 we present the element description. Since it is convenient to use different interpolations for the in-layer strains and for the transverse shear strains, the element [9] is formulated in its natural coordinate system (general curvilinear coordinates) and $\underline{g}_i$ are the usual covariant base vectors,

$$ \underline{g}_i = \frac{\partial\, {}^0\underline{x}}{\partial\, r_i} \tag{5} $$

with ${}^0\underline{x}$ from (1) and the following relations

$$ g_{ij} = \underline{g}_i \cdot \underline{g}_j \tag{6} $$

$$ \underline{g}^i = g^{ij}\ \underline{g}_j \tag{7} $$

$$g^{ij} = \frac{D^{ij}}{|J|^2} \tag{8}$$

where $i, j = 1, 2, 3$, D^{ij} is the cofactor of the tern g_{ij} in the matrix of the metric tensor and $|J|$ is the determinant of the Jacobian matrix at the point considered.

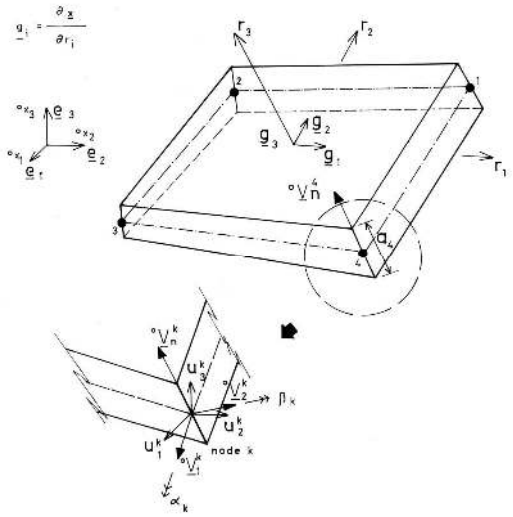


Figure 2: Four node shell element

Following the A-I-Z description for any point with natural coordinates (r_1, r_2,r_3) the cartesian coordinates at a time t, are:

$${}^t x_i = h_k \; {}^t x_i^k \; + \frac{r_3}{2} h_k \, a_k \, {}^t V_{ni}^k \tag{9}$$

and the incremental displacements from the undeformed configuration to the deformed one,

$$u_i = \; h_k \, u_i^k \; + \frac{r_3}{2} \, h_k \, a_k (-\alpha_k \, {}^t V_{2i}^k + \beta_k \, {}^t V_{1i}^k) \tag{10}$$

In the natural coordinate system, the strain tensor can be written as:

$$\underline{\underline{\varepsilon}} = \widetilde{\varepsilon}_{ij} \;\; \underline{g}^i \, \underline{g}^j \tag{11}$$

where $\underline{g}^i$ are the contravariant base vectors in convected coordinates, $\underline{g}^i \, \underline{g}^j$ the tensorial product between two contravariant vectors and $\widetilde{\varepsilon}_{ij}$ are the covariant components of Green Lagrange strain tensor

$$\widetilde{\varepsilon}_{ij} = \frac{1}{2} ({}^t \underline{g}_i \cdot {}^t \underline{g}_j - {}^0 \underline{g}_i \cdot {}^0 \underline{g}_j) \tag{12}$$

where

$$ {}^{0}\underline{g}_i = \frac{\partial\, {}^{0}\underline{x}}{\partial r_i} \tag{13} $$

and

$$ {}^{t}\underline{g}_i = \frac{\partial\,({}^{0}\underline{x} + \underline{u}\,)}{\partial r_i} \tag{14} $$

Neglecting non-linear terms in (12) the covariant components of the infinitesimal strain tensor are given by

$$ \widetilde{\varepsilon}_{ij} = \frac{1}{2}\left(\frac{\partial\,\underline{u}}{\partial\, r_i}\cdot\frac{\partial\,\underline{x}}{\partial\, r_j} + \frac{\partial\,\underline{x}}{\partial\, r_i}\cdot\frac{\partial\,\underline{u}}{\partial\, r_j}\right) \tag{15} $$

In the MITC4 formulation [9] the following strain interpolations are used:

·the in-layer strain components, $\widetilde{\varepsilon}_{11}$, $\widetilde{\varepsilon}_{22}$ and $\widetilde{\varepsilon}_{12}$, are directly calculated from the displacement / rotation interpolations using the kinematic relations.

·the transverse shear strains are interpolated using the following functions (see Figure 3)

$$ \widetilde{\varepsilon}_{13} = \frac{1}{2}(1+r_2)\,\widetilde{\varepsilon}_{13}{}^{DI}_{A} + \frac{1}{2}(1-r_2)\widetilde{\varepsilon}_{13}{}^{DI}_{C} $$

$$ \widetilde{\varepsilon}_{23} = \frac{1}{2}(1+r_1)\widetilde{\varepsilon}_{23}{}^{DI}_{D} + \frac{1}{2}(1-r_1)\widetilde{\varepsilon}_{23}{}^{DI}_{B} \tag{16} $$

In the above equations we indicate with the notation $\widetilde{\varepsilon}_{ij}{}^{DI}_{P}$ the covariant strain components calculated at the sampling point P from the displacement/rotation interpolation

At any point inside the element, a local Cartesian system, with base vectors $\widehat{\underline{e}}_i$ $(i = 1, 2, 3)$ is defined, and the components, $\widehat{C}^{mnop}$ are obtained by degenerating the $3D$ constitutive tensor to impose the simultaneous satisfaction of

$$ \widehat{\tau}_{33} = 0 \;\text{ and }\; \widehat{\varepsilon}_{33} = 0 \tag{17} $$

In the convected coordinates, the constitutive tensor is obtained using the transformation

$$ \widetilde{C}^{ijkl} = (\underline{g}^i\cdot\widehat{\underline{e}}_m)(\underline{g}^j\cdot\widehat{\underline{e}}_n)(\underline{g}^k\cdot\widehat{\underline{e}}_o)(\underline{g}^l\cdot\widehat{\underline{e}}_p)\;\widehat{C}^{mnop} \tag{18} $$

where

$$ \widehat{\underline{e}}_1 = \frac{\underline{g}_2\times\widehat{\underline{e}}_3}{\left|\underline{g}_2\times\widehat{\underline{e}}_3\right|} \tag{19} $$

and,

$$ \widehat{\underline{e}}_2 = \widehat{\underline{e}}_3\times\;\widehat{\underline{e}}_1 \tag{20} $$

hence

$$ \widetilde{\tau}^{ij} = \widetilde{C}^{ijkl}\widetilde{\varepsilon}_{kl} \tag{21} $$

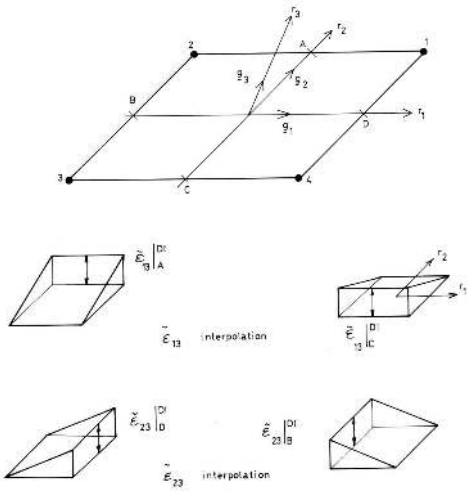


Figure 3: Transverse shear strain interpolations

where $\underline{\underline{\tau}}$ is the Cauchy stress tensor.

It is important to point out that the choice of the interpolation for the transverse shear strain components is the key assumption in the MITC formulation.

This element does not lock and does not contain spurious rigid modes. It also satisfies the Patch Test. For plate problems, this element have been mathematically analyzed (see [3] and [8]). Unfortunately, mathematical results when these methods are applied to shells are not known yet, and numerical testing is used. Some preliminary results in the mathematical analysis of MITC elements have been developed by Malinen [13] and Pitkaranta [15].

The low order MITC4 element improves the performance of the standard bilinear element considerably, and the gain is more important in the bending dominated case [15]. Attempting to have a successful formulation capable to model many different deformation states of a shell different treatments of the in-layer strains can be introduced in the membrane state case. In this way, one of the first approach, was adding incompatible modes to the displacement interpolation [2]. Simo and Armero [16] presented a class of mixed assumed strain methods that allows the development of low order elements with enhanced accuracy for coarse meshes. Another approach is to adapt quadrilateral 2-D finite elements, just as the hybrid element of Pian and Sumihara [14] or the QMITC element proposed by Dvorkin and Vassolo [11]. In next section we describe the formulation of a new shell element obtained adapting the interpolations of the QMITC, which is also based on the technique of mixed interpolation of tensorial components.

3 The new shell element

We present a 4-node shell element based on the method of mixed interpolation of tensorial components, which uses the MITC4 interpolations for the shear components of the strain tensor. Instead of evaluating the in-layer strain components from the displacement interpolations, a different approach is used which consists of adapting the formulation proposed in [11] for a quadrilateral 2-D finite element, the QMITC. This element overcame many of the drawbacks of the standard displacement based quadrilateral element and it can exactly represent a state of plane stress bending [11].

We use the displacement/rotation interpolations of the A-I-Z shell element, the transverse shear strains are interpolated using Eqs. (16) and the in-layer, $\widetilde{\varepsilon}_{11}$, $\widetilde{\varepsilon}_{22}$ and $\widetilde{\varepsilon}_{12}$ strains following the QMITC interpolations [11].

At any point inside the element with convective coordinates (r_1, r_2, r_3), we consider the surface $r_3 = r_3^*$, and the incremental displacements,

$$\underline{u} = \overline{h}_k \, \underline{u}^k + \frac{r_3^*}{2} \, \overline{h}_k \, a_k (-\alpha_k \, {}^0\underline{V}_2^k + \beta_k \, {}^0\underline{V}_1^k) \tag{22}$$

where $1 \leq k \leq 5$. Like in the QMITC element we consider an extra node in the center as shown in Figure 4 and then, the degrees of freedom corresponding to node 5 are condensed. The interpolations functions $\overline{h}_k$ are the corresponding to five node isoparametrical finite elements, i.e.

$$\overline{h}_k = h_k - \frac{1}{4}\overline{h}_5 \tag{23}$$

$$\overline{h}_5 = (1 - {r_1}^2) \;\; (1 - {r_2}^2) \tag{24}$$

and $h_k(r_1, r_2)$, the usual two dimensional interpolation functions corresponding to node $1 \leq k \leq 4$.

On this surface, the strain tensor can be written in the form

$$\underline{\varepsilon} = \widehat{\widetilde{\varepsilon}}_{11} \underline{\widehat{\widetilde{g}}}^1 \underline{\widehat{\widetilde{g}}}^1 \; + \widehat{\widetilde{\varepsilon}}_{22} \underline{\widehat{\widetilde{g}}}^2 \underline{\widehat{\widetilde{g}}}^2 + \widehat{\widetilde{\varepsilon}}_{12} \, (\underline{\widehat{\widetilde{g}}}^1 \underline{\widehat{\widetilde{g}}}^2 + \underline{\widehat{\widetilde{g}}}^2 \underline{\widehat{\widetilde{g}}}^1)$$

where, in this case, the covariant and contavariant base vectors are

$$\underline{\widehat{\widetilde{g}}}_i = \underline{g}_i \;\; \rfloor_{r_1 = r_2 = 0, r_3 = r_3^*} \tag{25}$$

and

$$\underline{\widehat{\widetilde{g}}}^i = \underline{g}^i \;\; \rfloor_{r_1 = r_2 = 0, r_3 = r_3^*} \tag{26}$$

We emphasize that an approximation is introduced in the above formulation since for non-flat elements $\underline{\widehat{\widetilde{g}}}_1$ and $\underline{\widehat{\widetilde{g}}}_2$ not necessarily belong to the tangent plane in the points used for the numerical integration, Gauss points r_i^*.

Considering, as we did before, the covariant components of the Green-Lagrange strain tensor in curvilinear coordinates (See Eq. (15))

$$\widetilde{\varepsilon}_{ij} = \frac{1}{2}(\frac{\partial \underline{u}}{\partial r_i}.\underline{g}_j \quad + \underline{g}_i \quad .\frac{\partial \underline{u}}{\partial r_j}) \tag{27}$$

where the covariants base vectors $\underline{g}_i$ were introduced in Eq. (5), and using the transformation laws we obtain the components in the the new system of coordinates,

$$\widehat{\widetilde{\varepsilon}}_{ij} = \widetilde{\varepsilon}_{lm} \quad (\widehat{\underline{g}}_i.\underline{g}^l) \; (\underline{g}^m.\widehat{\underline{g}}_j) \tag{28}$$

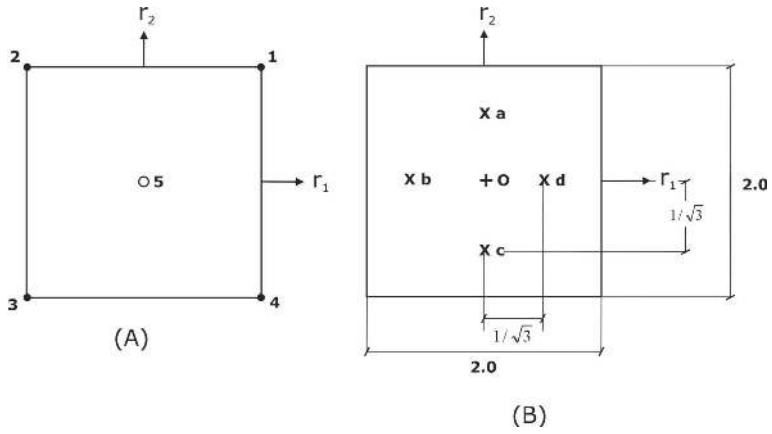


Figure 4: Nodes used for (A) displacement (B) strain interpolation

Using Eq. (27) the base contravariants vectors are calculated at the points o, a, b, c and d on the surface, and then the strain tensor components, $\widetilde{\varepsilon}_{11}$, $\widetilde{\varepsilon}_{22}$ and $\widetilde{\varepsilon}_{12}$ at the same points are evaluated (see Figure 4).

With the transformation (28) components in the base $\widehat{\widetilde{g}}$ are obtained and then in-layer components are calculated using the following interpolations

$$\widehat{\widetilde{\varepsilon}}_{11} = \widehat{\widetilde{\varepsilon}}_{11}\rfloor_o^{DI} + \frac{\sqrt{3}}{2}(\widehat{\widetilde{\varepsilon}}_{11}\rfloor_d^{DI} - \widehat{\widetilde{\varepsilon}}_{11}\rfloor_b^{DI}) \; \frac{|J_0|}{|J|} r_1 + \frac{\sqrt{3}}{2}(\widehat{\widetilde{\varepsilon}}_{11}\rfloor_a^{DI} - \widehat{\widetilde{\varepsilon}}_{11}\rfloor_c^{DI}) \; \frac{|J_0|}{|J|} r_2 \tag{29}$$

$$\widehat{\widetilde{\varepsilon}}_{22} = \widehat{\widetilde{\varepsilon}}_{22}\rfloor_o^{DI} + \frac{\sqrt{3}}{2}(\widehat{\widetilde{\varepsilon}}_{22}\rfloor_d^{DI} - \widehat{\widetilde{\varepsilon}}_{22}\rfloor_b^{DI}) \; \frac{|J_0|}{|J|} r_1 + \frac{\sqrt{3}}{2}(\widehat{\widetilde{\varepsilon}}_{22}\rfloor_a^{DI} - \widehat{\widetilde{\varepsilon}}_{22}\rfloor_c^{DI}) \frac{|J_0|}{|J|} r_2 \tag{30}$$

and

$$\widehat{\widetilde{\varepsilon}}_{12} = \widehat{\widetilde{\varepsilon}}_{12}\rfloor_o^{DI} \tag{31}$$

where J and J_0 are the element jacobians at (r_1, r_2) and $(0, 0)$ respectively, in both cases on the surface $r_3 = r_3^*$.

Finally components $\widetilde{\varepsilon}_{11}$, $\widetilde{\varepsilon}_{22}$ and $\widetilde{\varepsilon}_{12}$ are obtained in the curvilinear system using the relation

$$\widetilde{\varepsilon}_{ij} = \widehat{\widetilde{\varepsilon}}_{lm}\ (\underline{g}_l \cdot \widehat{\widetilde{\underline{g}}}^i)(\widehat{\widetilde{\underline{g}}}^j \cdot \underline{g}_m) \tag{32}$$

Next, the shear components of the strain tensor, $\widetilde{\varepsilon}_{13}$ and $\widetilde{\varepsilon}_{23}$, are interpolated as in MITC4 shell element.

It should be noted that the QMITC4 shell element has five nodes, and five degrees of freedom per node, but the ones corresponding to the center node are condensed assuming that

$$\widetilde{u}_3^5 = h_k \widetilde{u}_3^k \quad 1 \le k \le 4 \tag{33}$$

where $\widetilde{u}_3$ are the displacement in the $\underline{g}_3$direction defined in Eq. (5). Therefore, the resulting element has four nodes, as the MITC4 shell element.

Using the definition of the Green-Lagrange strain tensor and the above interpolations the following expressions are obtained:

$$\widetilde{\varepsilon}_{11}\rfloor_o^{DI} = \frac{1}{4}\,{}^0\widehat{\widetilde{\underline{g}}}_1 \cdot (\underline{u}^1 - \underline{u}^2 - \underline{u}^3 + \underline{u}^4) + \frac{r_3^*}{8}\,{}^0\widehat{\widetilde{\underline{g}}}_1 \cdot [a_1(-\alpha_1\ {}^0\underline{V}_2^1 + \beta_1\ {}^0\underline{V}_1^1)$$

$$-a_2(-\alpha_2\ {}^0\underline{V}_2^2 + \beta_2\ {}^0\underline{V}_1^2) - a_3(-\alpha_3\ {}^0\underline{V}_2^3 + \beta_3\ {}^0\underline{V}_1^3) + a_4(-\alpha_4\ {}^0\underline{V}_2^4 + \beta_4\ {}^0\underline{V}_1^4)] \tag{34}$$

$$\widetilde{\varepsilon}_{22}\rfloor_o^{DI} = \frac{1}{4}\,{}^0\widehat{\widetilde{\underline{g}}}_2 \cdot (\underline{u}^1 + \underline{u}^2 - \underline{u}^3 - \underline{u}^4) + \frac{r_3^*}{8}\,{}^0\widehat{\widetilde{\underline{g}}}_2 \cdot [a_1(-\alpha_1\ {}^0\underline{V}_2^1 + \beta_1\ {}^0\underline{V}_1^1)$$

$$+a_2(-\alpha_2\ {}^0\underline{V}_2^2 + \beta_2\ {}^0\underline{V}_1^2) - a_3(-\alpha_3\ {}^0\underline{V}_2^3 + \beta_3\ {}^0\underline{V}_1^3) - a_4(-\alpha_4\ {}^0\underline{V}_2^4 + \beta_4\ {}^0\underline{V}_1^4)] \tag{35}$$

$$\widetilde{\varepsilon}_{12}\rfloor_o^{DI} = \frac{1}{8}\,{}^0\widehat{\widetilde{\underline{g}}}_2 \cdot (\underline{u}^1 - \underline{u}^2 - \underline{u}^3 + \underline{u}^4) + \frac{1}{8}\,{}^0\widehat{\widetilde{\underline{g}}}_1 \cdot (\underline{u}^1 + \underline{u}^2 - \underline{u}^3 - \underline{u}^4) +$$

$$\frac{r_3^*}{16}\,{}^0\widehat{\widetilde{\underline{g}}}_2 \cdot [a_1(-\alpha_1\ {}^0\underline{V}_2^1 + \beta_1\ {}^0\underline{V}_1^1) - a_2(-\alpha_2\ {}^0\underline{V}_2^2 + \beta_2\ {}^0\underline{V}_1^2) - a_3(-\alpha_3\ {}^0\underline{V}_2^3 + \beta_3\ {}^0\underline{V}_1^3) +$$

$$a_4(-\alpha_4\ {}^0\underline{V}_2^4 + \beta_4\ {}^0\underline{V}_1^4)] + \frac{r_3^*}{16}\,{}^0\widehat{\widetilde{\underline{g}}}_1 \cdot [a_1(-\alpha_1\ {}^0\underline{V}_2^1 + \beta_1\ {}^0\underline{V}_1^1) +$$

$$a_2(-\alpha_2\ {}^0\underline{V}_2^2 + \beta_2\ {}^0\underline{V}_1^2) - a_3(-\alpha_3\ {}^0\underline{V}_2^3 + \beta_3\ {}^0\underline{V}_1^3) - a_4(-\alpha_4\ {}^0\underline{V}_2^4 + \beta_4\ {}^0\underline{V}_1^4)] \tag{36}$$

$$\widetilde{\varepsilon}_{11}\rfloor_a^{DI} = \frac{1}{4}\mu_1\ {}^0\widehat{\widetilde{\underline{g}}}_1^a \cdot \{(\underline{u}^1 - \underline{u}^2) + \frac{r_3^*}{2}[a_1(-\alpha_1\ {}^0\underline{V}_2^1 + \beta_1\ {}^0\underline{V}_1^1)$$

$$-a_2(-\alpha_2\ {}^0\underline{V}_2^2 + \beta_2\ {}^0\underline{V}_1^2)] + \frac{1}{4}\mu_2\ {}^0\widehat{\widetilde{\underline{g}}}_1^a \cdot \{(\underline{u}^4 - \underline{u}^3) +$$

$$\frac{r_3^*}{2}[-a_3(-\alpha_3\ {}^0\underline{V}_2^3 + \beta_3\ {}^0\underline{V}_1^3) + a_4(-\alpha_4\ {}^0\underline{V}_2^4 + \beta_4\ {}^0\underline{V}_1^4)] \tag{37}$$

$$\widetilde{\varepsilon}_{22}\rfloor_a^{DI}=\frac{1}{4}\mu_3\ {}^0\widehat{\underline{g}}_2^a\cdot\{(\underline{u}^1+\underline{u}^2)+\frac{r_3^*}{2}[a_1(-\alpha_1\ {}^0\underline{V}_2^1+\beta_1\ {}^0\underline{V}_1^1)+$$

$$a_2(-\alpha_2\ {}^0\underline{V}_2^2+\beta_2\ {}^0\underline{V}_1^2)]-\frac{1}{4}\mu_4\ {}^0\widehat{\underline{g}}_2^a\cdot\{(\underline{u}^4+\underline{u}^3)+\frac{r_3^*}{2}[a_3(-\alpha_3\ {}^0\underline{V}_2^3+\beta_3\ {}^0\underline{V}_1^3)+$$

$$a_4(-\alpha_4\ {}^0\underline{V}_2^4+\beta_4\ {}^0\underline{V}_1^4)]\}-\mu\ {}^0\widehat{\underline{g}}_2^a\cdot r_3^*a_5(-\alpha_5\ {}^0\underline{V}_2^5+\beta_5\ {}^0\underline{V}_1^5)-2\mu\ {}^0\widehat{\underline{g}}_2^a\cdot a_5\underline{u}^5 \tag{38}$$

$$\widetilde{\varepsilon}_{12}\rfloor_a^{DI}=\frac{1}{8}\mu_1\ {}^0\widehat{\underline{g}}_2^a\cdot\{(\underline{u}^1-\underline{u}^2)+\frac{r_3^*}{2}[a_1(-\alpha_1\ {}^0\underline{V}_2^1+\beta_1\ {}^0\underline{V}_1^1)$$

$$-a_2(-\alpha_2\ {}^0\underline{V}_2^2+\beta_2\ {}^0\underline{V}_1^2)]\}+\frac{1}{8}\mu_2\ {}^0\widehat{\underline{g}}_2^a\cdot\{(\underline{u}^4-\underline{u}^3)+\frac{r_3^*}{2}[-a_3(-\alpha_3\ {}^0\underline{V}_2^3+\beta_3\ {}^0\underline{V}_1^3)+$$

$$a_4(-\alpha_4\ {}^0\underline{V}_2^4+\beta_4\ {}^0\underline{V}_1^4)]\}+\frac{1}{8}\mu_3\ {}^0\widehat{\underline{g}}_1^a\cdot\{(\underline{u}^1+\underline{u}^2)+\frac{r_3^*}{2}[a_1(-\alpha_1\ {}^0\underline{V}_2^1+\beta_1\ {}^0\underline{V}_1^1)+$$

$$a_2(-\alpha_2\ {}^0\underline{V}_2^2+\beta_2\ {}^0\underline{V}_1^2)]\}-\frac{1}{8}\mu_4\ {}^0\widehat{\underline{g}}_1^a\cdot\{(\underline{u}^4+\underline{u}^3)+\frac{r_3^*}{2}[a_3(-\alpha_3\ {}^0\underline{V}_2^3+\beta_3\ {}^0\underline{V}_1^3)+$$

$$a_4(-\alpha_4\ {}^0\underline{V}_2^4+\beta_4\ {}^0\underline{V}_1^4)]\}-\mu^0\widehat{\underline{g}}_1^a\cdot\frac{r_3^*}{2}a_5(-\alpha_5\ {}^0\underline{V}_2^5+\beta_5\ {}^0\underline{V}_1^5)-\mu^0\widehat{\underline{g}}_1^a\cdot a_5\underline{u}^5 \tag{39}$$

where the coefficients μ_k correspond to the displacement derivatives $\frac{\partial u}{\partial r_i}$ and the interpolation functions, $\overline{h}_k$, at points o, a, b, c and d, respectively $\mu=\frac{1}{\sqrt{3}}$, $\mu_1=1+\mu$, $\mu_2=1-\mu$, $\mu_3=1+2\mu$ and $\mu_4=1-2\mu$. Similar expressions are obtained for $\widetilde{\epsilon}_{ij}$ at points b, c and d.

4 Numerical tests

4.1 Convergence

In this section we study the numerical behavior of the new element, achieving the following objectives:

- show that the element converges, that is to say that is consistent and stable [19].

- examine solutions it provides to some linear problems in order to gain insight into the element performance by comparing its behavior against MITC4.

In order to check the consistency of the formulation, the Patch Test with the mesh shown Figure 5 was used, and in all cases the transverse displacements, rotations and stresses exactly agreed with the analytical results [9].

In the first analysis (Figure 6) the mesh was loaded with the constant moment and a constant curvature i.e. linear distributions of rotations was obtained. The transverse displacements predicted by the model were, as expected, those of Kirchhoff-Love plate theory.

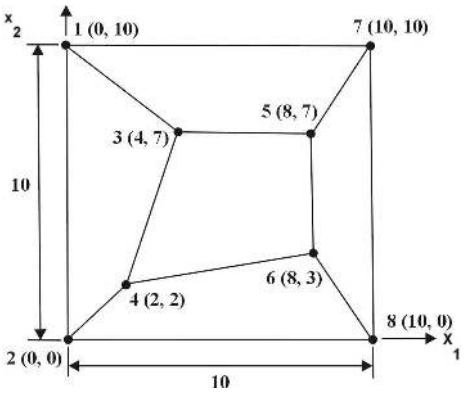


Figure 5: Patch Test mesh

In the second analysis the rotational degrees of freedom were deleted and the mesh was subjected to shear forces. As expected, a linear distribution of transverse displacement was obtained.

In the third analysis the mesh was subjected to an external twisting moment. In the thin plate analysis, constant curvatures were obtained in both plate directions and the transverse displacements agreed with the analytical thin plate theory solution.

Finally, it should be noted that the Patch Test is passed for the three membrane constant stress states.

For the new element stability analysis, the eigenvalues of the stiffness matrices of undistorted and distorted elements were calculated. In all cases, the element displayed the six rigid body modes and no spurious zero energy modes.

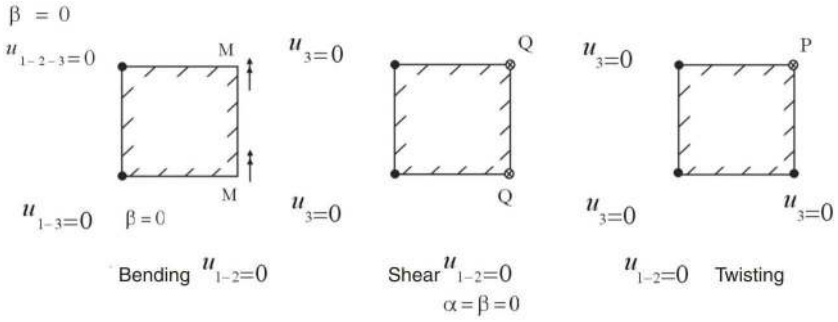


Figure 6: Patch Tests E=2.1 10^6, $\nu = 0.3$, thickness =1, $\frac{1}{1000}$

4.2 Numerical examples

We have performed various numerical tests to study the predictive capabilities of the new element, for both, plates and shells, with undistorted and distorted meshes. In this section we present the results corresponding to a few selected examples: Cook's membrane problem, a pinched cylinder, and a cylinder shell subjected to dead weight (Scordelis-Lo shell). We demonstrate the performance of the QMITC4 formulation and make a comparison with the MITC4 element.

Cook's membrane problem

A trapezoidal plate is clamped on one end and subjected to a distributed in-plane bending load on the other end, as shown in Figure 7. This problem has a considerable amount of shear deformation and is a good test of an element's ability to model membrane dominated situations. A finite element converged solution of 23.91 [17] is used to normalize the results, which are listed in Table 1. The material properties are $E = 1$, $\nu = 0.33$ and thickness $h = 1$. Good performance of the proposed element for a coarse mesh can be observed. Numerical results obtained using the incompatible modes formulation [17] or the interpolation for the membrane field inspired in the treatment of Pian and Sumihara [18] are almost identical to the ones obtained with QMITC4 element.

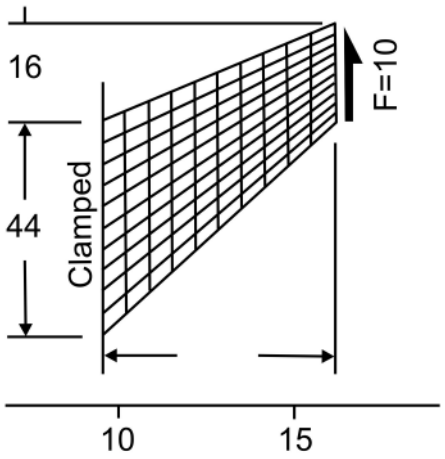


Figure 7: Cook's membrane problem

Pinched cylinder

A thin circular cylinder of length L, radius R, and thickness h with two pinching vertical forces P at the middle section as shown in Figure 8 is frequently used to test shell elements. The cylinder is restrained by two rigid diaphragms at the end and it is modelled using one octant

Table 1

N	$\frac{u_{z,MITC4}}{u_z}$	$\frac{u_{z,QMITC4}}{u_z}$
4	0.78	0.96
8	0.95	1.01
12	1.00	1.00

and applying appropiate symmetry boundary conditions. The material properties are $E = 10.5$ 10^6 and $\nu = 0.3$.

In Table 2 convergence of both elements is analyzed, with different $N \times N$ uniform meshes. It can be observed that for coarse meshes the QMITC4 element yields more accurate solutions than the ones obtained with MITC4, even if incompatible modes are added. As both elements converge to the analytical solution, the results tend to show less difference when the mesh is refined. ($\widehat{w}_{c,AN} = -164.24$ series solution by Lindberg et.al. [9], $\widehat{w}_c = \frac{w_c E h}{P}$)

In Ref. [9] the MITC4 solution is also compared with the 16-isoparametric element, which requires a fairly number of degrees of freedom to predict the response of the cylinder accurately.

Table 2

mesh	degrees of freedom	$\frac{\widehat{w}_{c,MITC4}}{\widehat{w}_{c,AN}}$	$\frac{\widehat{w}_{c,QMITC4}}{\widehat{w}_{c,AN}}$
5×5	130	0.51	0.54
12×12	756	0.89	0.92
14×14	1022	0.90	0.93
20×20	2060	0.96	0.97
24×24	2952	0.97	0.98

A cylindrical shell. Scordelis-Lo roof

This test problem is widely used for the evaluation of shell finite element procedures. The geometry of the mid-surface and the boundary conditions are described in Figure 9. The loading is a constant distributed vertical force (its dead weight) . The thickness is taken as constant over the whole structure. Due to symmetry the computational domain can be taken as one fourth of the whole shell (indicated with A, B, C and D in Figure 9).

The material properties are $E = 3 \times 10^6$, $\nu = 0$ and the analytical solution in B is $u_z = -3.6$. In Ref. [9] the numerical solution obtained with MITC4 element is compared with the values calculated using two 16-node shell elements and also DKT elements, showing the considerably predictive capability of this 4-node element.

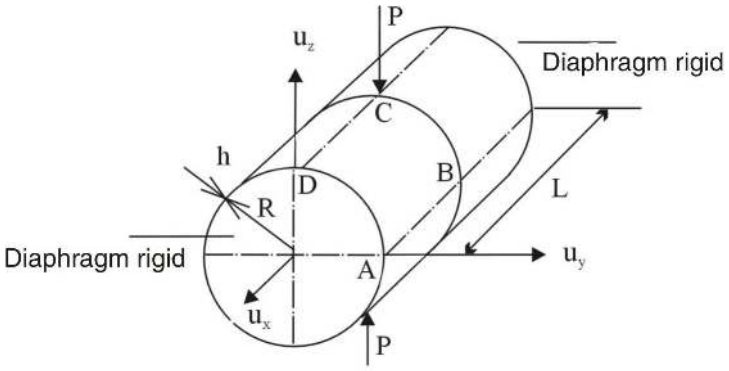


Figure 8: Pinched cylinder $\frac{R}{h} = 100$, $\frac{L}{R} = 2$

In Table 3, the results for the displacement at point B using both, QMITC4 and MITC4 elements are compared. In each uniform mesh were employed of $N \times N$ elements, and QMITC4 performs slightly superior to MITC4 element. It should be pointed out that in this case excellent results are also obtained when incompatible modes are introduced for membrane interpolations (99 % of the final solution is captured with N=6).

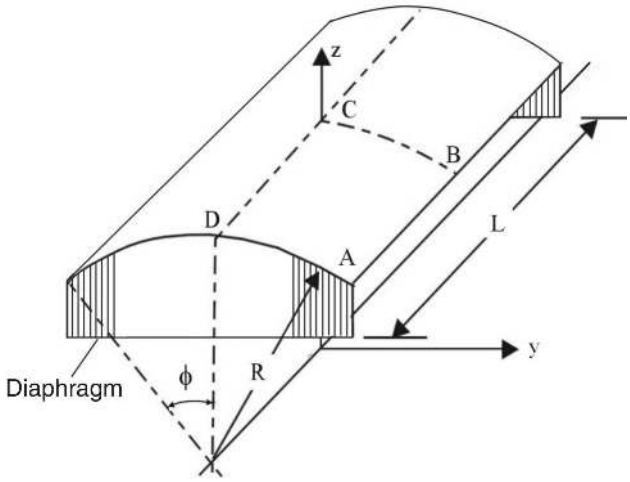


Figure 9: Scordelis-Lo shell R=300, L=600, Pe=0.208333, ϕ=40°, h=3

5 Conclusions

A four node shell element has been presented which -as the MITC4 element- is formulated using three-dimensional continuum mechanics theory (is not restricted by application of a specific shell

Table 3

N	degrees of freedom	$\frac{u_{z,MITC4}}{u_z}$	$\frac{u_{z,QMITC4}}{u_z}$
6	196	0.97	1.02
8	342	0.98	1.01
14	1020	0.99	1.00

theory) and mixed interpolation of tensorial components. It is obtained modifying the in-layer strain components using an interpolation based on the QMITC element. The shell element developed is reliable, does not lock and does not contain spurious rigid body modes so, it has good predictive capability in the analysis of thick and thin shells. In membrane dominated cases the comparison with MITC4 solutions using coarse meshes is most encouraging. Nevertheless, alternative approaches of the membrane strains could be implemented and analyzed in the future.

Acknowledgments. I like to express my gratitude to E. N. Dvorkin, for his support, encouragement and valuable suggestions.

References

[1] S. Ahmad, B. M. Irons, and O. C. Zienkiewicz. Analysis of thick and thin shells structures by curved finite elements. *Int. J. Num. Meth. in Eng.*, 2:419–451, 1970.

[2] K. J. Bathe. *Finite Element Procedures in Engineering Analysis*. Prentice-Hall, Englewood Cliffs, New Jersey, 1982.

[3] K. J. Bathe and F. Brezzi. On the convergence of a four-node plate bending element based on Reissner-Mindlin plate theory and a mixed interpolation. *MAFELAP V (J.R. Witheman, ed.)*, 1985.

[4] K. J. Bathe and E. N. Dvorkin. A four-node plate bending element based on Reissner-Mindlin plate theory and a mixed interpolation. *Int. J. Num. Meth. in Eng.*, 21(367-383), 1985.

[5] K. J. Bathe and E. N. Dvorkin. A formulation of general shell elements – the use of mixed interpolation of tensorial components. *Int. J. Num. Meth. in Eng.*, 22:697–722, 1986.

[6] K. J. Bathe, E. N. Dvorkin, and L. W. Ho. Our discrete Kirchhoff and isoparametric shell elements - an assessment. *Computers & Structures*, 16:89–98, 1983.

[7] D. Chapelle and K. J. Bathe. *The Finite Element Analysis of Shells-Fundamentals*. Springer-Verlag, Berlin Heidelberg, 2003.

[8] R. Durán and E. Liberman. On mixed finite element methods for the Reissner-Mindlin plate model. *Math. of Comp.*, 58(198):561–573, 1992.

[9] E. N. Dvorkin and K. J. Bathe. A continuum mechanics based four-node shell element for general nonlinear analysis. *Engng. Computations*, 1:77–88, 1984.

[10] E. N. Dvorkin and K. J. Bathe. Análisis de estructuras laminares generales utilizando el método de elementos finitos. *Rev. Int. de Métodos Numéricos para Cálculo y Diseño en Ingeniería*, 3:23–52, 1987.

[11] E. N. Dvorkin and S. I. Vassolo. A quadrilateral 2d finite element based on mixed interpolation of tensorial components. *Engng. Computations*, 6:217–224, 1989.

[12] E.N. Dvorkin. Nonlinear analysis of shells using the MITC4 formulation. *Archives Comput. Meth Engng*, 2:1–50, 1995.

[13] M. Malinen. On the classical shell model underlying bilinear degenerated shell finite elements. *Int. J. Num. Meth. in Eng.*, 52:389–416, 2001.

[14] T. H. Pian and K. Sumihara. Rational approach for assumed stress finite elements. *Int. J. Num. Meth. in Eng.*, 20:1685–1695, 1984.

[15] J. Pitkaranta. Mathematical and historical reflections on the lowestorder finite element models for thin structures. Technical report, Helsinky University of Technology, Institute of Mathematics Research Reports, 2003.

[16] J. C. Simo and F. Armero. Geometric non-linear enhanced strain mixed method and the method of incompatible modes. *Int. J. Num. Meth. in Eng.*, 15:1413–1418, 1980.

[17] J. C. Simo and S. Rifai. A class of mixed assumed strain methods and the methods of incompatible modes. *Int. J. Num. Meth. in Eng.*, 29:1595–1638, 1990.

[18] J.C. Simo, D.D. Fox, and M.S. Rifai. On a stress resultant geometrically exact shell model. Part II: The linear theory; computational aspects. *Comp.Methods in Ap. Mech and Eng.*, 73:53–92, 1989.

[19] G. Strang and G. Fix. *An Analysis of the Finite Element Method*. Prentice Hall, 1973.